Proceedings of the 28th IEEE
EMBS Annual International Conference
New York City, USA, Aug 30-Sept 3, 2006

Wall Shear Stress Variations in Basilar Tip Aneurysms investigated with Computational Fluid Dynamics

Christof Karmonik, Goetz Benndorf, Richard Klucznik, Hani Haykal, and Charles M. Strother

Abstract—**Hemodynamics are thought to play an important role in the creation, thrombosis, recanalization, regrowth and re-bleeding of cerebral aneurysms treated by endovascular means. However, their exact role and interaction is unclear and warrants further study. Towards a systematic classification of the hemodynamics in intracranial aneurysms, we investigated the dependence of the values of the magnitude of the wall shear stresses in the vicinity of the aneurysm on varying inflow conditions in three basilar tip aneurysms.**

I. Introduction

The rupture of an intracranial aneurysm is a serious clinical event leading to a subarachnoid hemorrhage (SAH) with potential fatal outcome. Prevalence of SAH is 8 to 10 people in 100 000 persons per year [1] with a mortality of 25 % -50 %. Most deaths are due to the initial bleed and its immediate complications. Despite the need for a well-defined treatment plan, management of an unruptured intracranial aneurysm is still controversial. Possible options include observation, endovascular coiling or surgical clipping. Symptomatic unruptured aneurysms (causing ischemic events, seizures, headaches, cranial nerve palsy), in contrast to asymptomatic unruptured aneurysms, will most likely be treated. However, it is not clear which aneurysms will rupture. With an overall morbidity and mortality for treatment of unruptured aneurysms of about 11 % [2], the availability of a technique to determine risk of rupture for a specific intracranial aneurysm would be very beneficial. Recently, this has become more important, because recent advances in medical imaging techniques, such as 64 slice CT and MRI at 3T, have led to an increase in the number of incidental findings of unruptured intracranial aneurysms. While aneurysm size has been identified to be an important risk factor, this criterion can only serve as a statistical guideline and alone will not be sufficient to predict rupture. Other geometric factors such as aspect ratio or the ratio between aneurysm volume and neck area may play a role as well. Recent research results [3-11], indicate that hemodynamic factors may provide such a criterion.

In the last decade, the endovascular treatment (EVT) of intracranial aneurysms has become more popular, mainly because this minimally invasive procedure is associated with significant lower mortality and morbidity than the conventional neurosurgical approach involving clipping of the aneurysm [12, 13]. With the advent of new endovascular devices such as intracranial stents, balloons and new generations of coils, a combination of treatment options is now available. Despite these recent improvements, the anatomical results obtained by EVT are still inferior to those obtained by surgical clipping. Therefore, the question of durability of EVT and long term protection of patients is still to be answered.

Many important hemodynamic factors in intracranial aneurysms cannot currently be assessed directly by means of imaging mainly due to the small size and the tortuosity of intracranial vessels compared to the resolution limits of suitable imaging methods such as clinical MRI. However, it has been shown that computational fluid dynamics (CFD) methods can provide such critical information [3, 11]. Furthermore, a deeper understanding of the hemodynamics, studied with computational methods, may help to develop criteria that could become future indicators for recurrence, re-bleeding and re-canalization of the endovascular treated aneurysm, such as the hemodynamical AFI (aneurysm formation indicator) [14].

Systematic CFD studies are needed to understand the influence of variations in the boundary conditions on the biologically important hemodynamics parameters, especially the magnitude of the wall shear stress (WSS). In the present study, we therefore simulated steady and unsteady flow in computational meshes of three basilar tip aneurysms with varying inflow conditions.

II. Methods

A. Image Acquisition

Three dimensional digital subtraction angiography (3D DSA) image data of three basilar tip aneurysms were retrospectively obtained from imaging studies performed as part of diagnostic angiograms. The angiograms were acquired on interventional C-arm systems (Axiom Artis, Siemens Medical Solutions, Erlangen, Germany). Using the Siemens Leonardo image post-processing with the Inspace

Manuscript received April 3, 2006. C. Karmonik is a Research Scientist with The Methodist Hospital Research Institute, Houston, TX 77030 USA (phone: 713-441-1583; fax: 713-790-6474; ckarmonik@ tmh..tmc.edu.)

G. Benndorf is an Interventional Neuroradiologist with The Methodist Hospital Research Institute, Houston, TX 77030 USA (gbenndorf@ tmh..tmc.edu.)

R. Klucznik, H. Haykal and C.M. Strother are interventional Neuroradiologists with The Methodist Hospital, Houston, TX 77030 USA (cnollkamper@ tmh..tmc.edu.)

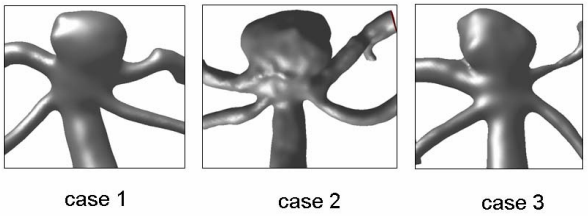

Fig. 1. Three dimensional surface reconstructions of the three basilar tip aneurysms (posterior view).

software, high-resolution 3D reconstructions of the acquired 3D DSA data were created. The isotropic spatial resolutions obtained were 0.1873 mm (case1), 0.0874 mm (case2) and 0.1352 mm (case 3). Images were then transferred to an off-line PC workstation for further manipulation.

After selecting a volume of interest containing the aneurysm and adjacent vessels, the image data was smoothed by convolution with a Gaussian kernel using VTK (Kitware Inc.). Visual inspection of the smoothed dataset and additional manipulations were then performed with Paraview (Kitware Inc.) and the final image data (fig. 1) was stored as a stereolithographic file for input into the meshing software GAMBIT (Fluent Inc.). Tetrahedral meshes were created with 133,646 volume elements for case 1; 87,263 volume elements for case 2 and 153,796 volume elements for case 3. The meshes were then imported into the CFD solver Fluent (Fluent Inc.). Three wall areas of interest were defined as follows: the aneurysm area (AA) as the wall area of the basilar tip (including the aneurysm), the basilar artery area (BAA) as the vessel wall area of a healthy section of the basilar artery and the aneurysm dome area (DA) located at the top of the aneurysm dome. Fig. 2 shows the computational mesh for case 1 and illustrates the location of the vessel wall areas.

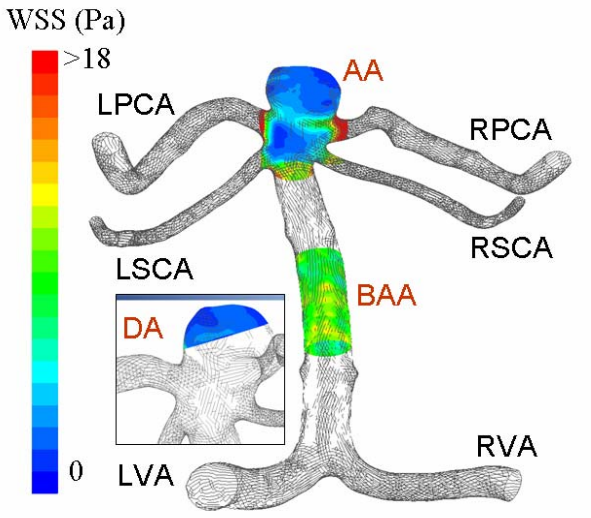

Fig. 2. Illustration of the wall areas AA, BAA and DA with contours of the wall shear stress magnitude at maximum flow in the unsteady case. (LPCA: left posterior cerebral artery, RPCA: right posterior cerebral artery, LSCA: left superior cerebellar artery, RSCA: right superior cerebellar artery, LVA: left vertebral artery, RVA: right vertebral artery).

Steady and unsteady simulations of blood flow were performed. With the converged solutions for the steady case, the simulations for the unsteady case were initialized. For case 2 and case 3, inflow was modeled as a velocity inlet realized as a cross section of the basilar artery. For case 1, inflow was modeled as two velocity inlets realized as cross sections of the right and left vertebral arteries.

For the steady case, average velocity values were used at the velocity inlets: 0.348 m/s for the basilar inlets [15], and

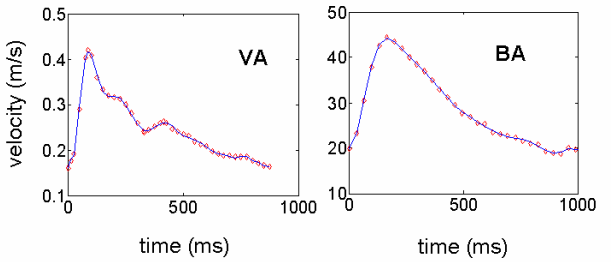

Fig. 3. Velocity waveforms utilized as unsteady boundary conditions. Left: average waveform for the vertebral artery, right: average waveform for the basilar artery.

0.52 m/s and 0.46 m/s for the right and left vertebral artery inlets, respectively [16]. For the unsteady case, an unsteady boundary condition of the velocity at the inlets was defined by polynomial interpolation derived from waveforms

TABLE I
CFD SIMULATION PARAMETERS

Case	Simulation
1	1: LVA 100 %, RVA 100 % 2: LVA 125 %, RVA 75 % 3: LVA 100 %, RVA 75 % 4: LVA 100 %, RVA 25 % 5: LVA 100 %, RVA 10 % 6: LVA 100 %, RVA closed
2	7: BA 100 % 8: BA 50 %
3	9: BA 100 % 10: BA 50 %

Percentage of inflow velocity at the velocity inlets.

measured with phase contrast MRI [17, 18] (fig. 3).

Blood was modeled as an incompressible Newtonian fluid with a density of 1000 kg/m^3 and a viscosity of 0.004 N/m^{2}s [5].

The time step for the unsteady simulations was chosen as 5 ms and the duration of the cardiac cycle was chosen as 820 ms when using the vertebral artery velocity flow waveform and 1000 ms when using the basilar artery velocity flow waveform. A total of 5 cardiac cycles were simulated and results were recorded from the 5th cardiac cycle to minimize any influence of transient effects.

The inlet boundary conditions were varied as shown in table 1.

III. RESULTS

Figure 4 shows the temporal variations of the WSS

magnitudes for the three wall areas AA, BAA and DA for case 1 with inflow from both vertebral arteries and inflow from only the left vertebral artery as well as for case 2 and case 3. From the WSS curves, the maximum, the minimum and the average values for the WSS magnitudes were determined. Relative average magnitudes of the WSS for AA and DA were derived by dividing the average value of the WSS magnitude for these wall areas by the WSS magnitude for the BAA. A time to maximum (tmax) was calculated as the time from the beginning of the cardiac cycle to the maximum of the WSS magnitude for each wall area. The values of these parameters are listed in table 2.

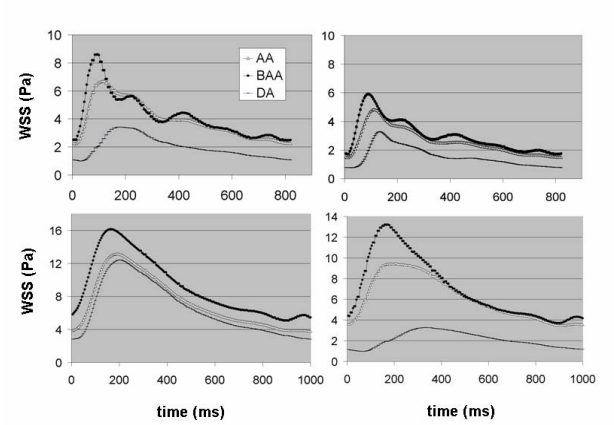

Fig. 4. Temporal variations of the wall shear stress magnitudes for the three vessel wall areas AA, BAA and DA over one cardiac cyle. Top left: case 1, simulation 1, inflow from both vertebral arteries, top right: case 1, simulation 6, inflow only from LVA. Bottom left: case 2, simulation 7, bottom right: case 3, simulation 9.

TABLE II
WSS PARAMETERS

SIM	area	Max	Min	Average	relative Average	tmax
1	AA	6.7	2.2	4.0	0.95	120
	BAA	8.6	2.5	4.2		95
	DA	3.4	1.0	2.0	0.48	180
2	AA	7.7	2.6	4.5	0.94	115
	BAA	9.7	2.8	4.8		85
	DA	4.1	1.2	2.4	0.50	160
3	AA	5.8	2.0	3.5	0.92	115
	BAA	7.7	2.2	3.8		95
	DA	2.8	0.8	1.7	0.45	190
4	AA	4.7	1.4	2.5	0.85	110
	BAA	5.8	1.7	2.9		85
	DA	2.2	0.5	1.1	0.36	140
5	AA	4.2	1.3	2.3	0.84	110
	BAA	5.3	1.6	2.7		85
	DA	1.9	0.4	0.9	0.34	135
6	AA	4.8	1.5	2.6	0.87	110
	BAA	5.9	1.7	3.0		90
	DA	3.3	0.7	1.5	0.51	135
7	AA	13.2	3.8	7.4	0.80	190
	BAA	16.1	5.1	9.2		165
	DA	12.4	2.8	6.5	0.71	200
8	AA	4.3	1.4	2.6	0.68	185
	BAA	6.5	2.1	3.8		165
	DA	3.3	0.7	1.8	0.48	235
9	AA	9.5	3.5	6.1	0.86	210
	BAA	13.2	3.7	7.1		160
	DA	3.3	1.0	2.1	0.30	330
10	AA	3.4	1.2	2.1	0.76	180
	BAA	5.2	1.5	2.8		160
	DA	0.7	0.2	0.4	0.15	440

SIM = simulation;, 1-6: case 1; 7-8: case 2; 9-10: case 3, units in Pa

IV. DISCUSSION

The temporal variations of the WSS magnitudes (fig. 4) show different dynamics for the three wall areas AA, BAA and DA in all three cases. In case 1, the WSS magnitude variations for BAA follow the variations of the input velocity waveform. The WSS curves for AA and DA are less pulsatile and also reach their maxima at different times (tmax in table 2). Qualitatively, the same behavior is observed for case 3. In contrast, for case 2, all three curves show the same dynamic behavior and differences in tmax are less pronounced. If inflow is only modeled by the LVA in case 1, the WSS magnitude curves for AA and DA regain some pulsatility.

Variations in the inflow conditions result in changes of the relative average WSS magnitude for the wall areas AA and DA, with the relative average of the WSS for AA varying from 95 % to 84 % for case 1; from 80 % to 68 % for case 2 and from 86 % to 76 % for case 3 and with the relative average of the WSS for DA varying from 50 % to 34 % for case 1, from 71 % to 48 % for case 2 and from 30 % to 15 % for case 3. While the overall variations in tmax for BAA and AA are relatively small in each case, higher variations in tmax for DA are noted.

Recent CFD simulations on intracranial aneurysms suggest that low WSS magnitudes may be one of the main factors underlying the degeneration of the aneurysm wall [3, 11]. A WSS of about 2.0 Pa is assumed to be suitable for maintaining the structure of arterial vessels and a WSS lower than 1.5 Pa will degenerate endothelial cells via the apoptotic cell cycle [19]. The correct simulation of the WSS therefore appears to be of high importance in CFD simulations if information about growth or rupture of an intracranial aneurysm should be derived from these simulations.

The results of our study demonstrate that not only the

absolute values but also the relative values of the WSS magnitude obtained at different wall segments in the basilar system using CFD techniques may strongly depend on the inflow conditions. In addition, also the time to maximum of the WSS curves varies with the inflow parameters. These variations suggest a high sensitivity of CFD simulations of the basilar system to the inflow conditions. To model the hemodynamics in intracranial aneurysm accurately, it seems therefore necessary to not only obtain high-resolution geometric information but also to use accurate flow information of the parent artery proximal to the intracranial aneurysm.

REFERENCES

[1] Linn FHH, Rinkel GJE, Algra A, van Gijn J. Incidence of subarachnoid haemorrhage—the role of region, year and rate of computed tomography—a meta-analysis. Stroke 1996; 27: 625–9.

[2] Wiebers DO, Whisnant JP, Huston J 3rd, Meissner I, Brown RD Jr, Piepgras DG, Forbes GS, Thielen K, Nichols D, O'Fallon WM, Peacock J, Jaeger L, Kassell NF, Kongable-Beckman GL, Torner JC; International Study of Unruptured Intracranial Aneurysms Investigators. Unruptured intracranial aneurysms: natural history, clinical outcome, and risks of surgical and endovascular treatment.Lancet. 2003 Jul 12;362(9378):103-10.

[3] Shojima M, Oshima M, Takagi K, Torii R, Hayakawa M, Katada K, Morita A, Kirino T. Magnitude and role of wall shear stress on cerebral aneurysm: computational fluid dynamic study of 20 middle cerebral artery aneurysms. Stroke. 2004 Nov;35(11):2500-5.C. J. Kaufman, Rocky Mountain Research Lab., Boulder, CO, private communication, May 1995.

[4] Hoi Y, Meng H, Woodward SH, Bendok BR, Hanel RA, Guterman LR, Hopkins LN. Effects of arterial geometry on aneurysm growth: three-dimensional computational fluid dynamics study.J Neurosurg. 2004 Oct;101(4):676-81.M. Young, *The Techincal Writers Handbook.* Mill Valley, CA: University Science, 1989.

[5] Hassan T, Ezura M, Timofeev EV, Tominaga T, Saito T, Takahashi A, Takayama K, Yoshimoto T. Computational simulation of therapeutic parent artery occlusion to treat giant vertebrobasilar aneurysm.AJNR Am J Neuroradiol. 2003 Nov-Dec;24(10):2044-9.

[6] Jou LD, Quick CM, Young WL, Lawton MT, Higashida R, Martin A, Saloner D. Computational approach to quantifying hemodynamic forces in giant cerebral aneurysms. AJNR Am J Neuroradiol. 2003 Oct;24(9):1804-10.

[7] Imbesi SG, Knox K, Kerber CW. Aneurysm flow dynamics: alterations of slipstream flow for neuroendovascular treatment with liquid embolic agents. AJNR Am J Neuroradiol. 2004 Jan;25(1):63-8.S. P. Bingulac, "On the compatibility of adaptive controllers (Published Conference Proceedings style)," in *Proc. 4th Annu. Allerton Conf. Circuits and Systems Theory*, New York, 1994, pp. 8–16.

[8] Cebral JR, Lohner R. Efficient simulation of blood flow past complex endovascular devices using an adaptive embedding technique.IEEE Trans Med Imaging. 2005 Apr;24(4):468-76. W. D. Doyle, "Magnetization reversal in films with biaxial anisotropy," in *1987 Proc. INTERMAG Conf.*, pp. 2.2-1–2.2-6.

[9] Steinman DA, Milner JS, Norley CJ, Lownie SP, Holdsworth DW. Image-based computational simulation of flow dynamics in a giant intracranial aneurysm. AJNR Am J Neuroradiol. 2003 Apr;24(4):559-66.J. G. Kreifeldt, "An analysis of surface-detected EMG as an amplitude-modulated noise," presented at the 1989 Int. Conf. Medicine and Biological Engineering, Chicago, IL.

[10] Groden C, Laudan J, Gatchell S, Zeumer H. Three-dimensional pulsatile flow simulation before and after endovascular coil embolization of a terminal cerebral aneurysm.J Cereb Blood Flow Metab. 2001 Dec;21(12):1464-71. N. Kawasaki, "Parametric study of thermal and chemical nonequilibrium nozzle flow," M.S. thesis, Dept. Electron. Eng., Osaka Univ., Osaka, Japan, 1993.

[11] Jou LD, Wong G, Dispensa B, Lawton MT, Higashida RT,Young WL, and Saloner D. Correlation between Lumenal Geometry Changes and Hemodynamics in Fusiform Intracranial Aneurysms. AJNR Am J Neuroradiol 26:2357–2363, (2005)..

[12] Brilstra EH, Rinkel GJ, van der Graaf Y, et al. Treatment of intracranial aneurysms by embolization with coils: a systematic review. Stroke 1999; 30:470–476.

[13] Johnston SC, Dudley RA, Gress DR, et al. Surgical and endovascular treatment of unruptured cerebral aneurysms at university hospitals. Neurology 1999; 52:1799–1805.

[14] Mantha A, Karmonik C, Benndorf G, Strother CM, , Metcalfe R. Hemodynamics in a Cerebral Artery Before and After the Formation of an Aneurysm. AJNR Am J Neuroradiol, accepted (2006).

[15] Seitz J, Strotzer M, Schlaier J, Nitz WR, Volk M, Feuerbach S. Comparison between magnetic resonance phase contrast imaging and transcranial Doppler ultrasound with regard to blood flow velocity in intracranial arteries: work in progress.J Neuroimaging. 2001 Apr;11(2):121-8.

[16] Seidel E, Eicke BM, Tettenborn B, Krummenauer F. Reference values for vertebral artery flow volume by duplex sonography in young and elderly adults.Stroke. 1999 Dec;30(12):2692-6.

[17] Ford MD, Alperin N, Lee SH, Holdsworth DW, Steinman DA. Characterization of volumetric flow rate waveforms in the normal internal carotid and vertebral arteries. Physiol Meas. 2005 Aug;26(4):477-88. Epub 2005 Apr 29.

[18] Kato T, Indo T, Yoshida E, Iwasaki Y, Sone M, Sobue G. Contrast-enhanced 2D cine phase MR angiography for measurement of basilar artery blood flow in posterior circulation ischemia. AJNR Am J Neuroradiol. 2002 Sep;23(8):1346-51.

[19] Malek AM, Alper SL, Izumo S. Hemodynamic shear stress and its role in atherosclerosis JAMA. 1999 Dec 1;282(21):2035-42.